A Spectroscopic and Computational Study of the Neutral and Radical Cation Species of Conjugated Aryl-Substituted 2,5-Bis(2-thien-2-ylethenyl)thiophene-Based Oligomers

John C. Earles,[†] Keith C. Gordon,*[,†] David L. Officer,[‡] and Pawel Wagner[‡]

MacDiarmid Institute for Advanced Materials and Nanotechnology, Department of Chemistry, University of Otago, Dunedin, New Zealand, and Nanomaterials Research Centre and MacDiarmid Institute for Advanced Materials and Nanotechnology, Massey University, Private Bag 11222, Palmerston North, New Zealand

Received: February 26, 2007; In Final Form: May 24, 2007

A spectroscopic and computational study of a series of 2,5-bis(2-thien-2-ylethenyl) thiophene-based oligomers with a *para*-R-arylethenyl substituent is reported. The primary aim of this investigation is to increase understanding of how charge moves through these molecules by comparing the neutral and oxidized structures for each molecule. To this end, the B3LYP/6-31G(d) computational method was used to calculate the geometry and vibrational spectra for all molecules considered and their oxidation products. For vibrational data, mean absolute deviations for frequencies between experimental and theoretical results ranging from 2 to 18 cm^{-1} were obtained. Experimental Raman spectroscopy, in conjunction with calculated bond length analyses, was used to gain an insight into the position and delocalization of the charged defect on the oxidized oligomers. The relative frequencies of different ethylene stretching modes served as a particularly useful probe in this regard. It was found that the ethenyl spacers do not impede π-electron delocalization and, therefore, give rise to a longer conjugation length relative to the corresponding terthiophenes. Furthermore, the *para*-R-arylethenyl substituent was found to orientate the charged defect toward a specific region of the 2,5-bis(2-thien-2-ylethenyl)-thiophene conjugation path.

I. Introduction

Conjugated polymers, such as polythiophenes, have been extensively studied in recent years because of their potential use in plastic electronic devices such as photovoltaic cells and field effect transistors.[1,2] The rational design of materials such as these requires an understanding of their structural properties in both their neutral and active (charged) states. Oligothiophenes have proven to be useful models for ascertaining structural characteristics and extrapolating these to the corresponding polythiophene. In addition, it has been found that the oligothiophenes themselves provide the excellent conductive properties of the analogous polymer but are without the associated problems of polydispersity and lack of solubility and processibility.[3,4] A number of researchers have shown that sexithiophene can be used to obtain efficient thin film transistor devices.[5−8] The key active intermediate in these conductive materials are their charged species and for oligothiophenes, these are radical cations and dications (positive polarons and bipolarons in the analogous polymer).[9]

An interesting way to extend these systems is to alter their electronic properties through substitution either off the thiophene rings[10−12] or between adjacent thiophene moieties. Nonhomogeneous co-oligomers built up from different conjugated units have been shown to exhibit improved electroluminescent properties compared with their homogeneous analogues.[13−15] The electronic properties of oligomers are largely controlled by the delocalization of π-electrons.[16,17] For systems involving aromatic units, the extent of delocalization is moderated by the resonance energy of the aromatic rings and the inter-ring rotations.[17] The inclusion of ethylene bridges within oligothiophenes decreases the aromaticity of the thiophene rings and enhances the planarity of the oligomer.[18] This results in an increased effective conjugation length and π-electron delocalization, giving rise to a system with a decreased band gap and redox potential.[16]

All nondegenerate conjugated polymers have a preference for one particular bond alternation arrangement over the other. The more stable arrangement is termed the benzenoid form, and the less stable geometry is called the quinoid form.[1,2] Upon the oxidation of a polymer, the positive charge is coupled via a quinodal conjugation path to either an unpaired electron or another positive charge to give the polaron and bipolaron respectively. In this manner, the unfavorable bond arrangement is confined, allowing the favored benzenoid arrangement to predominate outside of this domain. As such, bond length analyses and vibrational spectroscopy are particularly useful in elucidating the location and extent of delocalization of the charged defect.[19]

Owing to complications associated with long chain polymers, it is necessary to look at a smaller system, namely the oligomer units from which they are constructed. These smaller structural units have well-defined chemical and spectroscopic characteristics that have proven in the past to be reliable models for better understanding the corresponding polymers.[20,21] This approach also enables the use of the computational methods, which would be impractical for larger polymers.

Ten molecules have been investigated and are divided into two separate groups (see Figure 1). Group I comprises 2,5-bis-(2-thien-2-ylethenyl)thiophenes in which the central thiophene group is substituted with a styryl group containing an electron donating or withdrawing substituent R. The four different R substituents within group I are, in order of strongest electron donor to strongest electron acceptor, as follows: −OMe > −H

[†] University of Otago.
[‡] Massey University.

10.1021/jp071596g CCC: $37.00
Published on Web 07/07/2007

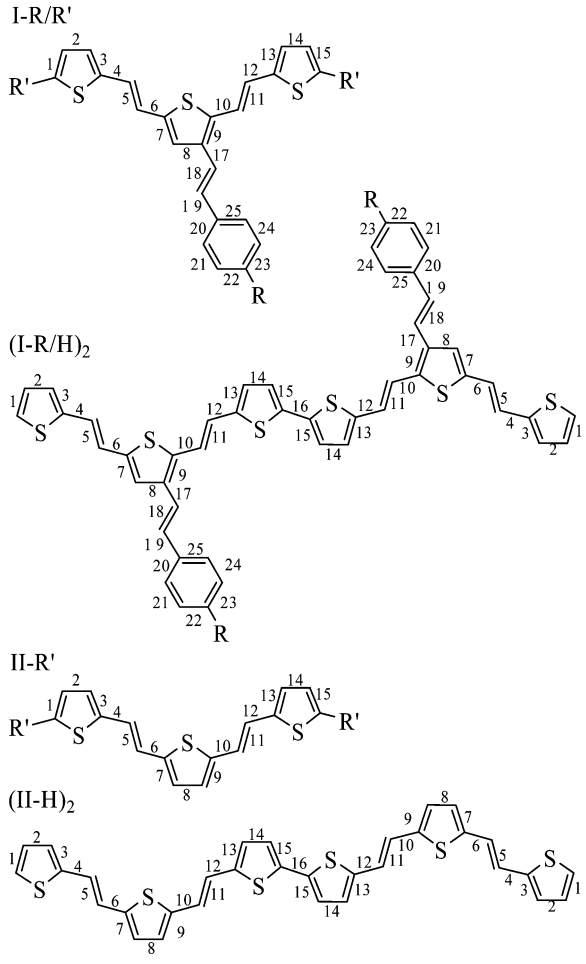

Figure 1. Adopted labeling scheme and bond numbering for all oligomers in this study.

> −CN > −NO_2. The group II molecules are the two parent 2,5-bis(2-thien-2-ylethenyl)thiophenes.

The polymerization of thiophene-based oligomers has been proposed to proceed via a radical−radical coupling mechanism involving the α positions of the terminal thiophene rings.[22] This is a facile process, such that terthiophene radical cation species only exist on the microsecond time scale[10,23,24] before undergoing rapid *σ*-dimerization to form the sexithiophene. However, the reaction does not proceed when methyl "end caps" are on the α-positions of the terminal thiophene rings. Each molecule in this study has been analyzed both with and without α,α′-end caps. The end-capped and open-ended molecules provide a means of examining the oxidized monomeric and dimeric species respectively. The adopted naming scheme and bond numbering systems are outlined in Figure 1.

II. Experimental Section

A. Materials. AR grade solvents and reagents were used for synthesis and were obtained from commercial sources. Dry THF was prepared by passing argon-degassed solvent through activated alumina columns. Column chromatography employed silica gel (0.032−0.063 mm, Merck Kieselgel 60) or the equivalent. Thin-layer chromatography (TLC) was performed using precoated silica gel plates (Merck Kieselgel 60F254). Either gravity or flash chromatography was used for compound purification.

B. Analytical Measurements. NMR spectra were recorded at 400.13/500.13 MHz (1H) using Brüker 400/500 Avance spectrometers running X-WIN-NMR software. The chemical shifts are relative either to tetramethylsilane (TMS) or to the residual proton signal in deuterated solvents ($CDCl_3$ δ 7.27). ^{13}C NMR shifts are relative to $CDCl_3$ (δ 77.0). Chemical shifts are reported as position (δ), multiplicity (s = singlet, d = doublet, t = triplet, q = quartet, dd = doublet of doublets, m = multiplet), relative integral, coupling constant (J in Hz), and assignment in $CDCl_3$ on a Bruker Avance 400 spectrometer using TMS as the internal standard. High-resolution mass spectrometry (HRMS) (fast-atom bombardment, FAB, and electron ionization, EI) was carried out using a Varian VG70−250S double-focusing magnetic-sector mass spectrometer. Samples analyzed by FAB-HRMS were supported on an *m*-nitrobenzyl alcohol matrix. The data were put through a MASSPEC II data system to give ±5 ppm error formulations on molecular ions. Major fragmentations are given as percentages relative to the base-peak intensity. Melting points are uncorrected.

C. Physical Measurements. All spectra were analyzed using GRAMS 5.0 (Galactic Industries). Infrared spectra were recorded from KBr discs on a Perkin-Elmer Spectrum BX FT-IR System using Spectrum v2.00 software. Each compound was scanned 32 scans times, with a resolution of 4.0 cm^{-1} and data point interval of 2.0 cm^{-1}. The Raman spectra of neutral compounds were recorded from solid powder samples using a Bruker IFS-55 FT-interferometer bench equipped with an FRA/106 Raman accessory and a LN_2-cooled Ge D418-T Raman detector. Radiation of 1064 nm from a Nd:YAG laser with an operating power of between 60 and 86 mW was utilized for Raman excitation. A total of 32 scans were recorded for each compound with a resolution of 4.0 cm^{-1} using OPUS software.

Solid films of the oxidized species were produced electrochemically on indium tin oxide (ITO) glass immersed in 1×10^{-4} mol L^{-1} solution of compound in 1×10^{-1} mol L^{-1} TBAP/acetonitrile. An oxidizing potential of 1 V was applied over deposition times of 3−5 min. The auxiliary electrode was a platinum mesh and a Ag/AgCl reference electrode was used. Resonance Raman spectra of the oxidized films were measured with an excitation wavelength of 752 nm using a system described previously.[25] Molecules II-Me and I-NO_2/Me did not form films because the oxidation products were too soluble. However, the resonance Raman spectrum of $(II\text{-}Me)^{\bullet+}$ was recorded with a 632 nm excitation wavelength using a system described previously.[26] Chemical oxidation was performed by adding 50 μL of 8×10^{-4} mol L^{-1} $Cu(ClO_4)_2$ in acetonitrile to 0.5 mL of 1×10^{-4} mol L^{-1} II-Me in acetonitrile.

D. Computational Studies. Optimized geometries, vibrational frequencies, and the corresponding IR and Raman intensities were calculated using the density functional theory (DFT) B3LYP/6-31G(d) method on the Gaussian 03 program.[27] The calculated frequencies have been scaled by a factor of 0.96, as recommended by Scott and Radom[28] to compensate for the tendency of DFT methods to overestimate force fields. All eigenvector diagrams were produced using the Molden software package.[29]

E. Synthesis. The syntheses of 2,5-bis(2-(thiophen-2-yl)-vinyl)-3-styrylthiophenes (I-R/H; R = OMe, H, CN, NO_2) have been described previously.[18] 2,5-Bis(2-(5-methylthiophen-2-yl)-vinyl)thiophene (II-Me) was synthesized according to a literature procedure.[30]

(*E,E*)*-2,5-Bis(2-(5-methylthiophen-2-yl)vinyl)thiophene-3-carbaldehyde.* 3-(5,5-Dimethyl[1,3]dioxan-2-yl)thiophene-2,5-dicarbaldehyde[18] (1.53 g, 6 mmol), (5-methylthien-2-yl)methyl-

triphenylphosphonium bromide[30] (8.16 g, 18 mmol), and DBU (7.50 g, 49 mmol) were dissolved in THF (75 mL), and the solution was refluxed under argon overnight. The reaction mixture was poured into aqueous HCl (150 mL, 10%) and extracted with dichloromethane (DCM). The organic phase was separated, dried over magnesium sulfate, and evaporated to dryness under a vacuum. The dark residue was purified on silica (ethyl acetate:hexane, 1:2). The fraction containing a mixture of protected and deprotected aldehyde was collected and dissolved in DCM (10 mL), and the resulting solution was stirred with trifluoroacetic acid (10 mL) and water (3 mL) for 1.5 h, then washed with aqueous sodium bicarbonate, and dried over magnesium sulfate. The solvent was removed, and the residue was purified on silica (DCM) and recrystallized from DCM-methanol to give fine red crystals of (*E*,*E*)-2,5-bis(2-(5-methylthiophen-2-yl)vinyl)thiophene-3-carbaldehyde (0.95 g, 44%), mp 141−142 °C. ^{1}H NMR (400 MHz): δ 10.06 (s, 1H, CHO), 7.56 (d, 1H, J = 16.0 Hz, vinyl-H), 7.21 (s, 1H, H4), 7.16 (d, 1H, J = 16.0 Hz, vinyl-H), 6.95 (d, 1H, J = 3.5 Hz, H3′), 6.92 (d, 1H, J = 15.8 Hz, vinyl-H), 6.85 (d, 1H, J = 3.5 Hz, H3″), 6.78 (d, 1H, J = 15.8 Hz, vinyl-H), 6.69 (dq, 1H, J = 3.5 and 0.7 Hz, H4′), 6.65 (dq, 1H, J = 3.5 and 0.7 Hz, H4″), 2.50 (d, 1H, J = 0.7 Hz, Me′), 2.48 (d, 1H, J = 0.7 Hz, Me″). ^{13}C NMR (100 MHz): δ 184.0, 150.1, 142.0, 140.3, 140.0, 139.7, 139.5, 136.6, 128.8, 127.3, 127.2, 126.3, 126.0, 123.8, 119.0, 116.5, 15.8, 15.7. MS (EI): 356 (100), 323 (13), 294 (11), 280 (10), 178 (9), 111 (9). HRMS (EI): found, 356.0368; requires for $C_{19}H_{16}OS_3$, 356.0363.

General Procedure for Wittig Condensation. 2,5-Bis(2-(5-methylthiophen-2-yl)vinyl)thiophene-3-carboxaldehyde (150 mg, 0.42 mmol), the appropriate phosphonium salt (0.5 mmol), and DBU (1.50 g, 9.8 mmols) were dissolved in THF (15 mL), and the solution was refluxed under argon overnight. The reaction mixture was poured into aqueous HCl (20 mL, 10%) and extracted with DCM. The organic phase was separated, dried over magnesium sulfate, and evaporated to dryness under vacuo. The dark residue was purified on silica (DCM) and recrystallized from DCM/methanol.

(*E,E,E*)-*(2,5-Bis(2-(5-methylthien-2-yl)vinyl)-3-(2-(4-methoxyphenyl)vinyl)thiophene (I-MeO/Me).* [(4-Methoxyphenyl)methyl]triphenylphosphonium bromide was used in the general Wittig condensation procedure above to give 55 mg (28%) of I-MeO/Me as irregular yellow crystals, mp 172−174 °C. ^{1}H NMR (400 MHz): δ 7.46−7.43 (m, 2H, Ar−H), 7.14 (s, 1H, H4), 7.10 (d, 1H, J = 15.5 Hz, vinyl-H), 7.07 (d, 1H, J = 16.0 Hz, vinyl-H), 6.95−6.83 (m, 8H, Ar−H + 4 × vinyl-H + H3′ + H3″), 6.66−6.64 (m, 2H, H4′ + H4″), 3.84 (s, 3H, OMe), 2.50 (d, 3H, J = 0.7 Hz, Me′), 2.48 (d, 3H, J = 0.7 Hz, Me″). ^{13}C NMR (100 MHz): δ 159.4, 140.7, 140.3, 139.9, 139.7, 139.6, 137.3, 136.4, 130.1, 129.2, 127.7, 126.7, 126.6, 126.0, 125.9, 124.5, 122.7, 122.2, 120.0, 118.3, 117.9, 114.2, 55.3, 15.70, 15.69. MS (EI, %): 460 (100), 349 (20), 339 (18), 217 (11), 111 (10). HRMS (EI, %): found, 460.0987; requires for $C_{27}H_{24}OS_3$, 460.0989.

(*E,E,E*)-*(2,5-Bis(2-(5-methylthien-2-yl)vinyl)-3-(2-(4-cyanophenyl)vinyl)thiophene (I-CN/Me).* [(4-Cyanophenyl)methyl]triphenylphosphonium bromide was used in the general Wittig condensation procedure above to give 122 mg (64%) of I-CN/Me as bright orange fine irregular crystals, mp 169−170 °C. ^{1}H NMR (400 MHz): δ 7−64-7.62 (m, 2H, Ar−H), 7.56−7.54 (m, 2H, Ar−H), 7.27 (d, 1H, J = 16.0 Hz, vinyl-H), 7.12 (s, 1H, H4), 7.05 (d, 1H, J = 15.5 Hz, vinyl-H), 6.96 (d, 1H, J = 15.5 Hz, vinyl-H), 6.93 (d, 1H, J = 15.5 Hz, vinyl-H), 6.90−6.83 (m, 2H, H3′ + H3″), 6.81 (d, 1H, J = 15.5 Hz, vinyl-H), 6.67−6.65 (m, 2H, H4′ + H4″), 2.50 (d, 3H, J = 0.7 Hz, Me′), 2.49 (d, 3H, J = 0.7 Hz, Me″). ^{13}C NMR (100 MHz): δ 141.9, 140.3, 140.26, 140.2, 140.0, 139.1, 135.9, 133.8, 132.5, 127.3, 127.2, 127.0, 126.7, 126.2, 126.0, 124.0, 123.5, 123.4, 123.2, 119.6, 118.0, 117.1, 110.3, 15.8, 15.7. MS (EI, %): 455 (100), 344 (10), 111 (24), 69 (10), 57 (12), 43 (11). HRMS (EI): found, 455.0835; requires for $C_{27}H_{21}NS_3$, 455.0836.

(*E,E,E*)-*(2,5-Bis(2-(5-methylthien-2-yl)vinyl)-3-(2-(4-nitrophenyl)vinyl)thiophene (I-NO$_2$/Me).* [(4-Nitrophenyl)methyl]triphenylphosphonium bromide was used in the general Wittig condensation procedure above to give 115 mg (58%) of I-NO$_2$/Me as fine red prisms, mp 208−210 °C. ^{1}H NMR (500 MHz): δ 8.22−8.21 (m, 2H, Ar−H), 7.62−7.61 (m, 2H, Ar−H), 7.35 (d, 1H, J = 16.1 Hz, vinyl-H), 7.15 (s, 1H, H4), 7.08 (d, 1H, J = 15.5 Hz, vinyl-H), 6.99 (d, 1H, J = 15.5 Hz, vinyl-H), 6.94 (d, 1H, J = 15.5 Hz, vinyl-H), 6.93 (d, 1H, J = 16.1 Hz, vinyl-H), 6.89 (d, 1H, J = 3.5 Hz, H3′), 6.85 (d, 1H, J = 3.5 Hz, H3″), 6.83 (d, 1H, J = 15.5 Hz, vinyl-H), 6.68 (dq, 1H, J = 3.5 and 0.7 Hz, H4′), 6.66 (dq, 1H, J = 3.5 and 0.7 Hz, H4″), 2.51 (d, 3H, J = 0.7 Hz, Me′), 2.50 (d, 3H, J = 0.7 Hz, Me″). ^{13}C NMR (100 MHz): δ 146.6, 144.0, 140.4, 140, 37, 140.2, 140.1, 140.0, 139.6, 135.8, 127.4, 127.1, 126.8, 126.7, 126.2, 126.0, 124.5, 124.2, 123.9, 123.6, 123.3, 119.6, 117.1, 15.8, 15.7. MS (EI, %): 475 (100), 445 (34), 256 (10), 149 (13), 129 (20), 97 (22), 91 (37), 83 (29), 69 (52), 57 (63), 43 (58). HRMS (EI): found, 475.0734; requires for $C_{26}H_{21}NO_2S_3$, 475.0734.

(*E,E,E*)- *and (E,E,Z)-(2,5-Bis(2-(5-methylthien-2-yl)vinyl)-3-(2-phenylvinyl)thiophene (I-H/Me).* (Phenylmethyl)triphenylphosphonium bromide was used in the general Wittig condensation procedure above to give 60 mg (33%) of a 92:8 ratio of an *E,E,E* and *E,E,Z* isomeric mixture of I-H/Me as fine orange irregular crystals, mp 125−132 °C. ^{1}H NMR (400 MHz): δ 7.53−7.50 (m, 2H, Ph−H), 7.39−7.36 (m, 3H, Ph−H), 7.20 (d, 1H, J = 16.2 Hz, vinyl-H), 7.16 (s, 1H, H4), 7.11 (d, 1H, J = 15.5 Hz, vinyl-H), 6.94 (d, 1H, J = 15.5 Hz, vinyl-H), 6.93 (d, 1H, J = 15.5 Hz, vinyl-H), 6.92 (d, 1H, J = 16.2 Hz, vinyl-H), 6.85 (d, 1H, J = 15.5 Hz, vinyl-H), 6.86−6.82 (m, 2H, H3′ + H3″), 6.66−6.64 (m, 2H, H4′ + H4″), 2.49 (d, 3H, J = 0.7 Hz, Me′), 2.48 (d, 3H, J = 0.7 Hz, Me″). ^{13}C NMR (100 MHz): δ 140.6, 140.2, 140.0, 139.8, 137.4, 137.2, 137.0, 129.6, 128.7, 127.7, 126.8, 126.4, 126.1, 126.0, 124.5, 122.8, 122.5, 120.3, 120.0, 117.8, 15.72, 15.70. MS (EI, %): 430 (100), 319 (10), 129 (11), 77 (10), 57 (12). HRMS (EI): found, 430.0884; requires for $C_{26}H_{22}S_3$, 430.0884.

III. Results and Discussion

A. Molecular Structure. The oligomers studied here have many degrees of freedom. As such, the particular conformation on which to perform computational analyses is an important consideration. The energy of a conformation is determined primarily by two opposing forces: steric effects and conjugation. Steric interactions between the thiophene rings are unfavorable and would result in a twisted structure if not for the decrease in energy imparted by planarity and the ensuing conjugation.[12] The inclusion of ethylene spacers minimizes steric interactions between the thiophene rings and increases effective conjugation length. Accordingly, the coplanarity of the thiophene rings are expected to be enhanced in II-H as compared with oligothiophenes.[31] The conformation used in these studies is a planar arrangement in which each ethylene C═C bond is in an *anti* disposition to the C═C of the neighboring thiophene ring (Figure 1). This is in accordance with crystal structure data reported on

a similar β-substituted thieneylenevinylene: (*E*,*E*)-3-(5,5-dimethyl[1,3]dioxin-2-yl)-2,5-bis(2-thien-2-ylvinyl)thiophene).[18] DFT studies of other thienylenevinylene oligomers have also found this anti conformation to be significantly more stable than the syn arrangement.[13,17] The orientation of the substituent for molecules of group I has been chosen to minimize steric interactions with the thienylenevinylene backbone.

In the case of the σ-dimers, a number of regio-isomers are possible depending on the orientation of the substituent groups with respect to each other; these are termed head-to-head, tail-to-tail, and head-to-tail. All discussion of σ-dimers concerns the head-to-head arrangement of the substituents; i.e., the arylethenyl substituents are both orientated toward the center of the dimer. This was selected as the lowest energy conformation following point energy calculations of the different substituent arrangements for $(\text{I-H/H})_2$ using the B3LYP/6-31G(d) method. Furthermore, we will show in this report that for the series of oxidized monomers $(\text{I-R/H})^{\bullet+}$, the free radical is orientated more toward the terminal α-C, and that gives rise to the head-to-head conformer upon dimerization.

Geometry optimizations have been performed on all molecules in their neutral state using the B3LYP/6-31G(d) method. The bond lengths clearly exhibit the single-double (long−short) bond alternation that is associated with Peierl's distortion and the resulting benzenoid resonance contributor. The degree of bond length alternation (Δ_{BL}) can be taken as a measure of effective conjugation length[15,17] and is defined as the average difference in the lengths of alternating single and double bonds. Comparing the bond lengths of the central thiophene ring for II-H and terthiophene itself, bonds 7 and 8 (Figure 1) are calculated as 1.384 and 1.412 Å, respectively, for II-H (Δ_{BL} = 0.028 Å) and the corresponding bonds within terthiophene have been calculated using the same method at 1.379 and 1.417 Å (Δ_{BL} = 0.038 Å).[32] The decrease in the bond length alternation of II-H relative to terthiophene indicates that the ethylene bridges serve to increase the effective conjugation length and therefore enhance the delocalization of π-electrons.

Both the shortest and longest bond distances are associated with the double and single bonds of the ethylene bridges respectively. For example, bonds 4−6 of II-H have been calculated at 1.442, 1.356, and 1.438 Å respectively, Δ_{BL} = 0.084 Å. The increase in the degree of bond length alternation relative to the thiophene moieties is indicative of the larger band gap associated with the ethylene moieties.[33−35]

The calculated bond lengths along the thienylenevinylene backbone (bonds 1−15 as detailed in Figure 1) are effectively equivalent for all group I molecules with or without end caps. Minor differences between the substituted molecules and II-H/II-Me occur adjacent to the substituent position. Bonds 8 and 9 are 0.016−0.021 Å longer in group I molecules compared to those of group II. This is because the additional resonance structures that involve the substituent impart more single bond character on bonds 8 and 9 (Figure 1).

B. Vibrational Spectra of Neutral Species. DFT vibrational calculations have been performed on all molecules in their neutral states to assess the reliability of the geometry optimizations and to identify significant Raman vibrational modes. The calculated Raman amplitudes were related to Raman band intensity for 1064 nm excitation, as used in the experimental measurements. No imaginary wavenumbers were observed for any of the compounds, consistent with a molecular geometry within an energy minimum.[36]

The correlation between the theoretical and experimental spectra is quantified with the mean absolute deviation (MAD) of the corresponding peak frequencies, measured in wavenumbers. The assessment criteria for this study were as follows: All peaks in the experimental spectra that are above a relative intensity of 20% have been identified and related to peaks in the equivalent theoretical spectrum based upon peak position and intensity patterns. A MAD approaching the spectrometer resolution of 4 cm^{-1} represents an excellent correlation between experimental and theoretical spectra. Analysis within this work has been restricted to within the 800−1800 cm^{-1} range because this regions contains the C−C and C═C stretching modes, which are particularly useful in the analysis of conjugated systems. Furthermore, in experimental studies no Raman bands of significant intensity are observed outside of this region. All experimental and theoretical intensities were normalized to the highest peak in the region of interest.

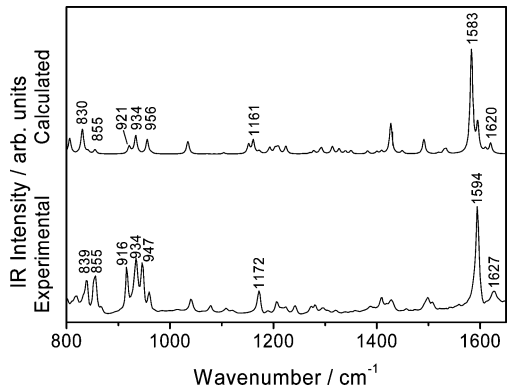

Figure 2. Experimental (bottom) and calculated (top) IR spectra for I-CN/H. The experimental spectrum was taken of a solid KBr disc, the theoretical spectrum was calculated using the B3LYP/6-31G(d) method.

TABLE 1: Mean Absolute Deviation (MAD) Data Derived from the Comparison of the Frequencies of Matched Bands in the Experimental and Theoretical Vibrational Spectra for All Molecules in This Study

	MAD	
molecule	IR (cm^{-1})	Raman (cm^{-1})
I-OMe/H	4	6
I-H/H	5	12
I-CN/H	6	8
I-NO_2/H	11	5
II-H	18	2
I-OMe/Me	5	9
I-H/Me	6	9
I-CN/Me	9	9
I-NO_2/Me	9	10
II-Me	12	6

The calculated and experimental IR spectra for I-CN/H are depicted in Figure 2, with the wavenumbers of all modes relevant to the calculation of the MAD indicated. In addition to the good correlation as quantified by the MAD, there is also a qualitative correlation in the peak intensity. The MAD data for all IR and Raman spectra are presented in Table 1. The MAD varies from 2 to 18 cm^{-1}, and the average value across the data set is 7 cm^{-1}. As such, the calculated geometries and vibrational frequencies for all compounds in their neutral states can be considered reliable models of the true systems.

The experimental Raman spectra are generally less complex than the IR spectra, as is typical of conjugated oligomers.[21] This suggests that the ethylene bridges do not interrupt the delocalization of π-electrons.[35] The calculated spectra are similarly uncomplicated, enabling an unequivocal correlation between experimental and theoretical data. This is explicit in the comparison of the experimental and theoretical Raman spectra

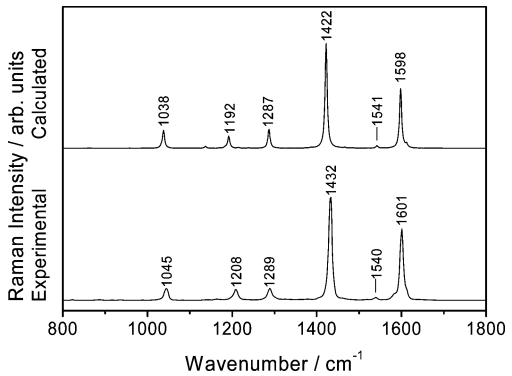

Figure 3. Experimental (bottom) and calculated (top) Raman spectra for II-Me. Experimental spectrum taken from solid state ($\lambda_{ex} = 1064$ nm), spectrum calculated using the B3LYP/6-31G(d) method.

for II-Me, which is depicted in Figure 3; the spectra are strikingly similar and give an accordingly small MAD of 6 cm^{-1}. The eigenvectors corresponding to the dominant bands are depicted in Figure 4 and will be referred to during the succeeding discussion on the Raman spectra of all molecules.

The Raman spectra of oligothiophenes are often characterized in terms of four main lines termed lines A, B, C and D.[16,34,35] Line A is primarily made up of the totally symmetric υ_{as}(C═C) of the outer thiophene rings, corresponding to the mode observed at 1540 cm^{-1} in the spectrum of II-Me (Figure 4). The mode decreases in frequency as the number of thiophene rings increases; the extent of the shift can be used as a parameter for measuring effective conjugation length.[16,21,35] Line A is observed for all molecules in this study except II-H. It is observed between 1532 and 1535 cm^{-1} for the remaining open-ended molecules (cf. 1558 cm^{-1} for terthiophene[21]) and between 1539 and 1545 cm^{-1} for all end-capped molecules (cf. 1546 cm^{-1} for end-capped terthiophene[37]). These data represent a decrease in the vibrational frequency of line A relative to the nonintercalated terthiophenes, indicating that the ethylene bridges serve to increase the effective conjugation length.

Line B is always very intense for thiophene-based oligomers and is composed of a fully in-phase symmetric υ_s(C═C) mode. This corresponds to the mode calculated at 1422 cm^{-1} for II-Me (Figure 4). Line B is observed from 1413 to 1419 cm^{-1} and 1428 to 1435 cm^{-1} for all open-ended and end-capped molecules, respectively. This increase in the vibrational frequency of line B associated with methyl end caps is similarly observed in the Raman spectra of non-ethylene bridged thiophenes. For example, line B is observed at 1463 cm^{-1} for open-ended terthiophene[21,38] and 1488 cm^{-1} for the end-capped terthiophene.[13,37] These data also indicate that the mode is at significantly lower wavenumber in the spectra of II-H and II-Me compared to the corresponding oligothiophenes. The ethylene bridging groups increase the effective conjugation length and act to mediate the bond length alternation present in the σ-bonded thiophene units. Thus the C═C double bonds that are active in the line B vibrational mode have a lower double bond character and therefore lower vibrational frequency in comparison to terthiophene.

Line D corresponds to the fully in-phase symmetric bending of the C−H bonds on the terthiophene rings and is assigned to the mode calculated at 1038 cm^{-1} for II-Me (Figure 4). Little structural information can be gleaned from line D, which is observed between 1043 and 1046 cm^{-1} for all molecules in this study. In contrast, line C is only observed for a few classes of oligomers[16] and is not observed in any of the Raman spectra obtained in this study.

The band observed at 1208 cm^{-1} in the Raman spectrum of II-Me (Figure 3) corresponds to the calculated mode at 1192 cm^{-1} (Figure 4). It is composed of a totally symmetric ν_{as}(C−C), primarily involving the central thiophene and the ethylene moieties. The band is consistent throughout the spectra of all the molecules studied here.

The Raman bands of II-Me observed experimentally at 1601 and 1289 cm^{-1} are characteristic of the ethylene moiety. The former has been assigned to the symmetric C═C stretch; the upshift in frequency relative to that of the thiophene C═C mode is consistent with the smaller bond length calculated for the ethylene double bond. The band situated at 1290 cm^{-1} has been assigned to C−H bending of the ethylene moiety.

The thiophene-based modes show only small deviations in frequency across all experimental Raman spectra. However, the ethylene stretch mode at approximately 1600 cm^{-1} splits into separate modes in the experimental Raman spectra of group I molecules. Substitution at the central thiophene ring lowers the symmetry of the molecule; this results in the two ethylene moieties of the thienylenevinylene backbone having different vibrational frequencies due to different spatial relationships with the substituent. Furthermore, the substituent itself has an ethylene moiety. The behavior of the ethylene modes is exemplified in the theoretical and experimental Raman spectra for I-CN/Me (Figure 5a,b). Three distinct bands are observed experimentally at 1594, 1612, and 1620 cm^{-1}. The calculated eigenvectors for the different ethylene stretching modes are depicted in Figure 6. The band observed experimentally at 1620 cm^{-1} evidently corresponds to that calculated at the same frequency, with the eigenvector centered on bond 18. Similarly, the band observed at 1612 cm^{-1} corresponds to the mode calculated at 1608 cm^{-1} and centered bond five. The two calculated modes at 1594 and 1581 cm^{-1} are constituted primarily by the stretching of bond 11. These differ in that they are symmetrically and asymmetrically coupled to the contraction of the phenyl ring respectively. These two calculated modes correspond to the broad and intense peak observed experimentally at 1594 cm^{-1}.

C. Raman Spectra of Oxidized Species. Having identified the key bands in the Raman spectra of the neutral species, it is possible to determine the corresponding vibrational modes in the Raman spectra of the doped oligomers and deduce structural information from any changes in frequency or intensity that occurs. The precise calculation of absolute intensities and frequencies is the domain of high-accuracy, small molecule calculations.[36] However, for larger oligomer systems the predictions of changes in spectra upon oxidation can be very effective.[13,34,39] If the experimentally observed shifts in frequency associated with oxidation (resulting from a benzenoid to quinoid transformation and/or σ-dimerization) are accurately predicted in the theoretical spectra, then the calculations can be regarded as reliable.[32] The relevant oxidized species upon which to perform vibrational calculations were selected in accordance with electrochemical and electronic absorption data that are not reported. All open-ended molecules exhibit evidence of σ-dimerization in oxidizing media and vibrational calculations have consequently been performed on the cationic dimers.

The analysis of the end-capped species, which do not form σ-dimers, is undertaken initially. The comparison between the experimental and theoretical Raman spectra of $(II\text{-}Me)^{\bullet+}$ is depicted in Figure 7. The calculations do not account for resonance enhancement and as such the intensity patterns of the two spectra are disparate; however, the correlation is still apparent. We now discuss the spectra in terms of the line A, B,

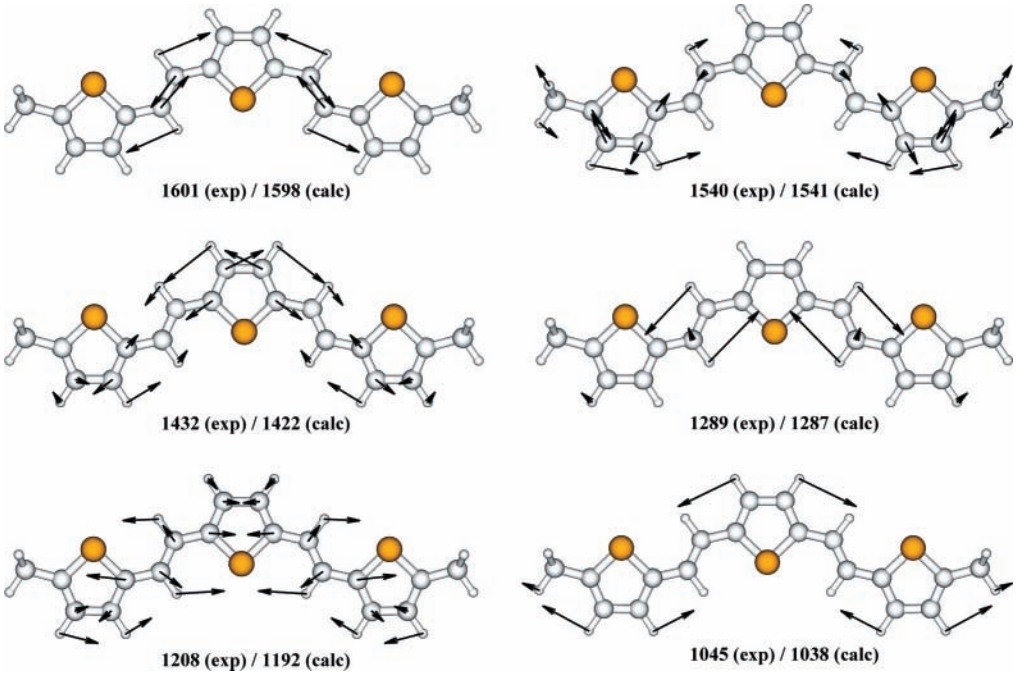

Figure 4. Schematic eigenvectors for the main Raman active vibrations of II-Me. The experimental (exp) and calculated (calc) values are given in cm^{-1}. The modes observed experimentally at 1540, 1432, and 1045 cm^{-1} correspond to lines A, B, and D, respectively, as defined in refs 16, 34, and 45. These diagrams were produced using the Molden software package.[29]

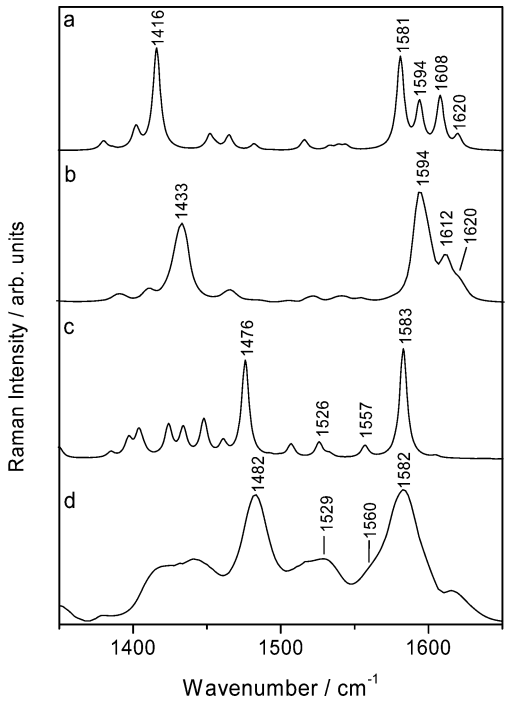

Figure 5. (a) Theoretical Raman spectrum for I-CN/Me, calculated using the B3LYP/6-31G(d) method. (b) The experimental Raman spectrum for I-CN/Me, taken from solid state (λ_{ex} = 1064 nm). (c) Theoretical spectrum for $(I\text{-}CN/Me)^{\bullet+}$, calculated using the B3LYP/6-31G(d) method. (d) Experimental spectrum for $(I\text{-}CN/Me)^{\bullet+}$, taken of a solid-state oxidized film using an excitation wavelength of 752 nm.

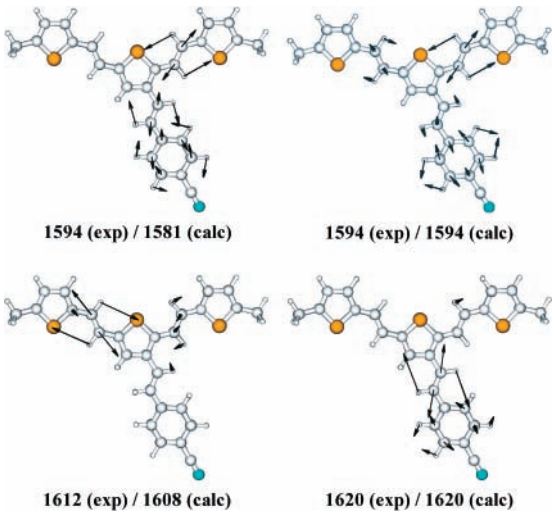

Figure 6. Schematic eigenvectors for the Raman active ethylene stretching modes of I-CN/Me, calculated at the B3LYP/6-31G(d) level (both values given in cm^{-1}). These diagrams were produced using the Molden software package.[29]

and D classification. The very weak band observed at 1507 cm^{-1} has been assigned to the line A mode, on the basis of the theoretical eigenvector which is calculated at 1499 cm^{-1}. The weak nature of this mode has been observed previously for similar oxidized thienylenevinylenes.[13] Line B is not observed in the Raman spectrum of $(II\text{-}Me)^{\bullet+}$. A two band feature is instead prominent at 1473 and 1448 cm^{-1}. Line D is observed as a weak absorption at 1056 cm^{-1}.

The band observed at 1568 cm^{-1} in the experimental spectrum of $(II\text{-}Me)^{\bullet+}$ has been assigned to the ethylene stretching mode, and the analogous mode in the spectrum of neutral II-Me is observed at 1601 cm^{-1} (Figure 3). The decrease in frequency upon oxidation is indicative of the benzenoid-to-quinoid geometrical distortion, as the double bond of the ethylene group gains more single bond character. This shift in frequency is accurately predicted with the bands calculated at 1555 and 1598 cm^{-1} for the theoretical spectra of $(II\text{-}Me)^{\bullet+}$ and II-Me, respectively. The ethylene δ_{C-H} bending mode is observed at 1284 cm^{-1} in the experimental spectrum of $(II\text{-}Me)^{\bullet+}$ and is predicted at 1276 cm^{-1}.

The theoretical and experimental Raman spectra for $(I\text{-}CN/Me)^{\bullet+}$ are depicted in Figure 5c,d respectively. Three separate

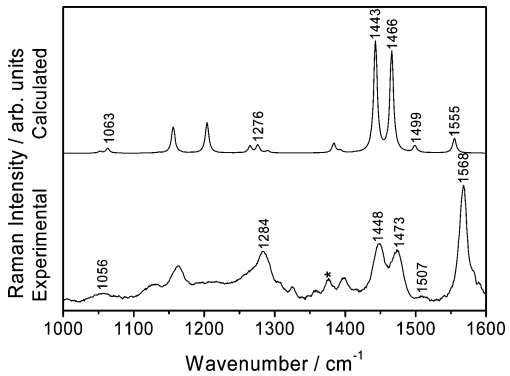

Figure 7. Experimental (bottom) and calculated (top) Raman spectra for $(II\text{-}Me)^{\bullet+}$. The experimental spectrum was taken from 1 mL of a 1×10^{-4} mol L^{-1} acetonitrile solution of II-Me, with 1×10^{-4} mL of 8×10^{-4} mol L^{-1} $Cu(ClO_4)_2$ in acetonitrile added. An excitation wavelength of 632 nm was used. The asterisk denotes a solvent band. The theoretical spectrum was calculated using the B3LYP/6-31G(d) method.

TABLE 2: Comparison between Ethylene Stretching Frequencies (cm^{-1}) for $(I\text{-}CN/Me)^{\bullet+}$ and I-CN/Me (Numbering System Depicted in Figure 1)

I-CN/Me		$(I\text{-}CN/Me)^{\bullet+}$		$\Delta\nu = \nu_{parent} - \nu_{oxidized}$		bond mode
expt	calc	expt	calc	expt	calc	is centered on
1620	1620	1582	1583	−38	−37	18
1612	1608	1560	1557	−52	−51	5
1594	1581	1529	1526	−65	−55	11

ethylene stretching modes are observed experimentally at 1582, 1560, and 1529 cm^{-1}. These correspond to calculated modes at 1583, 1557, and 1526 cm^{-1} respectively. The eigenvectors associated with these modes are entirely analogous to those of the corresponding neutral species I-CN/Me discussed previously (Figure 6); i.e., they are centered on bonds 18, 5, and 11 respectively.

Table 2 details the comparison between analogous ethylene stretching modes for I-CN/Me and $(I\text{-}CN/Me)^{\bullet+}$. The relative shift ($\Delta\nu = \nu_{parent} - \nu_{oxidized}$) of each vibrational mode upon oxidation can yield structural information pertaining to the location of the polaron. The ethylene stretch centered on bond 11 is observed at 1529 cm^{-1} in the experimental Raman spectrum of $(I\text{-}CN/Me)^{\bullet+}$. This constitutes a $\Delta\nu = -65$ cm^{-1} relative to the corresponding band in the spectrum of the neutral species. Therefore, within $(I\text{-}CN/Me)^{\bullet+}$, the polaron is orientated more toward bond 11 than bonds 5 and 18, which experience $\Delta\nu = -52$ and -38 cm^{-1}, respectively.

These results can be explained in terms of the two distinct conjugation paths within the oxidized oligomer. The polaron is predominantly located across the thienylenevinylene backbone. However, the arylethenyl substituent is conjugated with bonds 9−15 of the thienylenevinylene backbone, providing an additional resonance contributor that can harbor polaron structure. Both scenarios direct the polaron over bond 11, whereas competing resonance structures impart single bond character on bonds 5 and 18 separately.

Separate and distinct ethylene stretching modes are similarly observed for the σ-dimers that are formed upon the oxidation of open-ended molecules. This includes the oxidation product of the unsubstituted II-H, which we have concluded to be the bipolaron σ-dimer $(II\text{-}H)_2^{2+}$. One mode is centered on the outermost ethylene moieties and another on the innermost moieties, calculated at 1560 and 1547 cm^{-1}, respectively. The fact that there is only a small difference between the two frequencies is indicative of the delocalized nature of the

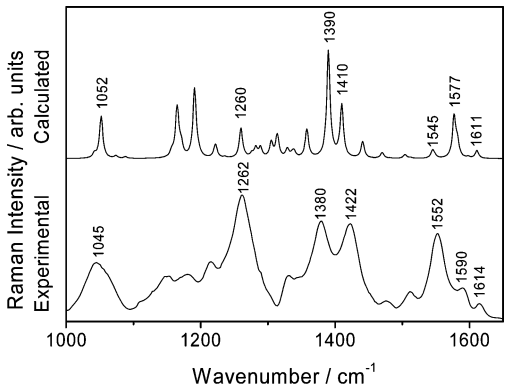

Figure 8. Experimental (bottom) and calculated (top) Raman spectra for $(I\text{-}NO_2/H)_2^{\bullet+}$. The experimental spectrum is that of the solid-state oxidized film using an excitation wavelength of 752 nm. The theoretical spectrum was calculated using the B3LYP/6-31G(d) method.

bipolaron. This is in agreement with the experimental resonance Raman spectrum in which a broad peak is observed at 1558 cm^{-1}.

All group I oxidation products are considered to be σ-dimers with a single positive charge, as opposed to the dicationic state considered for the σ-dimer of II-H. This is in accordance with electrochemical data that are not reported. The experimental and theoretical Raman spectra of the σ-dimer $(I\text{-}NO_2/H)_2^{\bullet+}$ are shown in Figure 8 and discussed below as a representative example. Although a comparison with the Raman spectrum of the neutral σ-dimer $(I\text{-}NO_2/H)_2$ would be ideal, these data are not available.

The two-peak feature in the Line B region is again observed at 1380 and 1422 cm^{-1}, line D is observed at 1045 cm^{-1}, and the ethylene δ_{C-H} bending mode is observed at 1262 cm^{-1}. Three distinct ethylene stretching modes are observed at 1552, 1590, and 1614 cm^{-1} in the experimental Raman spectrum of $(I\text{-}NO_2/H)_2^{\bullet+}$ (Figure 8). These correlate to the modes calculated at 1545, 1577, and 1611 cm^{-1} respectively, for which the eigenvectors are depicted in Figure 9. The differences in the observed frequencies of the three modes can be used to derive the location of the polaron in the same manner as above. Considering the vibrational mode associated with the two central ethylene moieties, the corresponding peak is observed experimentally at 1552 cm^{-1}, which is significantly lower than the stretching mode of the outer two ethenyl bonds, observed at 1590 cm^{-1}. This indicates that the polaron is more prominent toward the center of the thienylenevinylene backbone. The mode associated with the arylethenyl substituent is observed at 1614 cm^{-1} and shows negligible shift in frequency from the corresponding mode in the spectrum of the neutral monomer. This suggests that the substituent does not interact appreciably with the polaron; i.e., the polaron is situated almost exclusively along the thienylenevinylene backbone.

D. Bond Length Analysis. The vibrational data for both the neutral and oxidized species indicate that theoretical calculations have reliably predicted the structures of all species. Consequently, the comparison between the carbon−carbon bond lengths of a neutral oligomer and the corresponding oxidized species can be used to examine the position and delocalization of the charged defect. These data reveal the benzenoid-to-quinoid geometric distortion that occurs upon oxidation, where double bonds gain single bond character and vice versa within the confines of the charged defect. Bond length alternation diagrams (bond length versus bond number) are often utilized to depict these changes.[13,32−34,39,40]

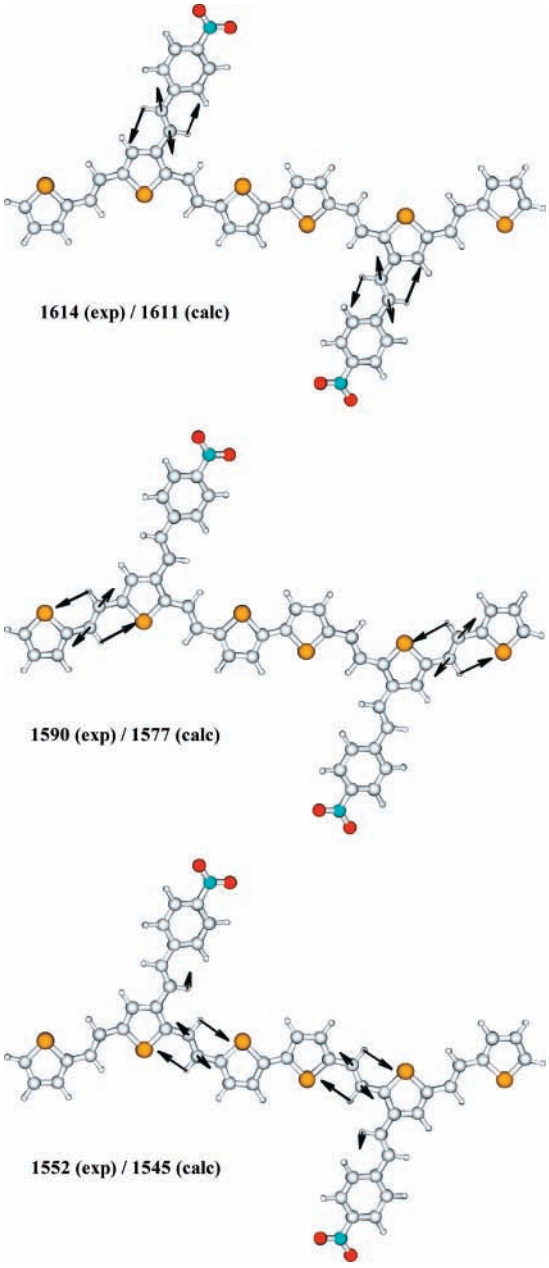

Figure 9. Schematic eigenvectors for the ethylene C=C stretch of $(I\text{-}NO_2/H)_2^{\bullet+}$, calculated at the B3LYP/6-31G(d) level (all values given in cm^{-1}). These diagrams were produced using the Molden software package.[29]

The discussion of the end-capped molecules, which remain as monomers upon oxidation, is undertaken initially. The bond length alternation diagram of II-Me and its charged species $(II\text{-}Me)^{\bullet+}$ is shown in Figure 10(a). This indicates that the formation of a quinoidal structural domain in the molecule is more pronounced toward the center of the conjugation path, indicating some bias of the charged defect to that region. This has previously been observed for a large number of thiophene-based oligomers.[13,32−34,39,40]

The bond alternation diagram for I-H/Me and $(I\text{-}H/Me)^{\bullet+}$ is presented (Figure 10b) to discuss the effects of the substituent. As with the unsubstituted $(II\text{-}Me)^{\bullet+}$, the polaron structure is extended across the entire thienylenevinylene backbone; however, the full quinoidal bond sequence is limited to bond 9 only, in comparison with bonds 7−9 in $(II\text{-}Me)^{\bullet+}$. This was likewise calculated for all group I molecules with end caps in their oxidized states.

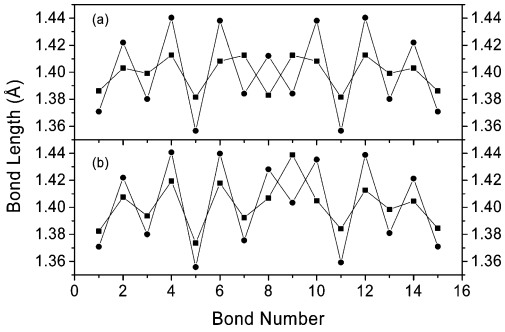

Figure 10. (a) Bond lengths for the thienylenevinylene backbone of II-Me (●) and $(II\text{-}Me)^{\bullet+}$ (■). (b) Bond lengths for the thienylenevinylene backbone of I-H/Me (●) and $(I\text{-}H/Me)^{\bullet+}$ (■). Calculated using the B3LYP/6-31G(d) method. The bond labeling system is shown in Figure 1.

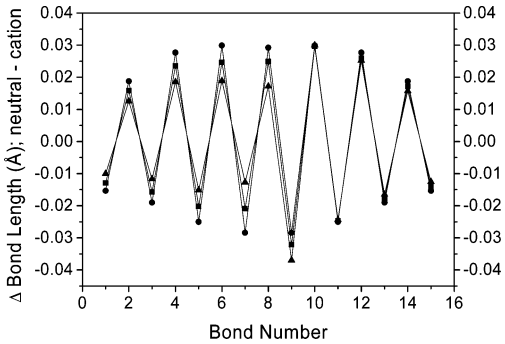

Figure 11. Change in bond lengths of the thienylenevinylene backbone upon oxidation of II-Me (●), $I\text{-}NO_2/Me$ (■), and II-OMe/Me (▲). Calculated using the B3LYP/6-31G(d) method. The bond labeling system is shown in Figure 1.

For the group I compounds, the effect of the β-substituents alters the nature of the polaron structure. The change in bond lengths (neutral minus oxidized) for bonds 17−19 of the arylethenyl substituent are largest for I-OMe/Me (+0.018, −0.013, and +0.019 Å respectively), the molecule with the most electron donating substituent. Conversely, the changes are the smallest for the molecule with the most electron withdrawing nitro group (+0.003, −0.002, and +0.001 Å). This result is entirely intuitive: the +I substituent is better able to donate electron density to the positive polaron and therefore can stabilize the charged defect by partially extending the structural distortion to the phenylethenyl substituent.[39]

The different inductive effects of the substituents are likewise reflected in the bond lengths of the thienylenevinylene backbone. Figure 11 depicts the changes in the bond lengths of the backbone that occur upon the oxidation of molecules II-Me, I-OMe/Me, and $I\text{-}NO_2/Me$ (the last two representing the two extremes of inductive effects within group I). The smallest changes in the length of bonds 1−8 are calculated for I-OMe/Me. This is because the electron donating methoxy arylethenyl substituent acquires much of the polaron structure. This in turn means that less of the polaron is localized along the thienylenevinylene backbone for $(I\text{-}OMe/Me)^{\bullet+}$. The larger changes in bond length observed for $I\text{-}NO_2/Me$ reflect the more electron withdrawing nature of the nitro phenylethenyl substituent.

Interestingly, the nature of the substituent has no significant effect on the lengths of bonds 10−15. Indeed, there is negligible difference in bond length between the substituted (I-OMe/Me and $I\text{-}NO_2/Me$) and unsubstituted (II-Me) molecules across this section of the thienylenevinylene backbone (Figure 11). These results echo the trends discussed previously in relation to the resonance Raman spectra: that the phenylethenyl substituent

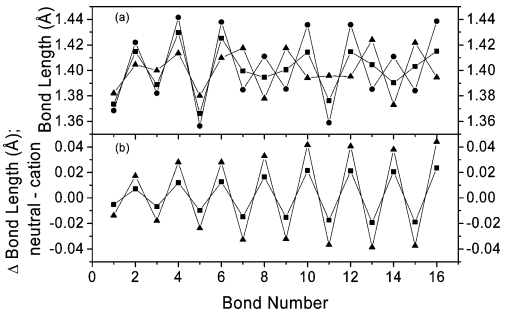

Figure 12. (a) Calculated bond lengths for the thienylenevinylene backbone of $(II\text{-}H)_2$ (●), $(II\text{-}H)_2^{\bullet+}$ (■) and $(II\text{-}H)_2^{2+}$ (▲). (b) Change in the thienylenevinylene backbone bond lengths relative to the neutral dimer $(II\text{-}H)_2$ for both $(II\text{-}H)_2^{\bullet+}$ (■) and $(II\text{-}H)_2^{2+}$ (▲). Calculated using the B3LYP/6-31G(d) method. The bond labeling system is shown in Figure 1.

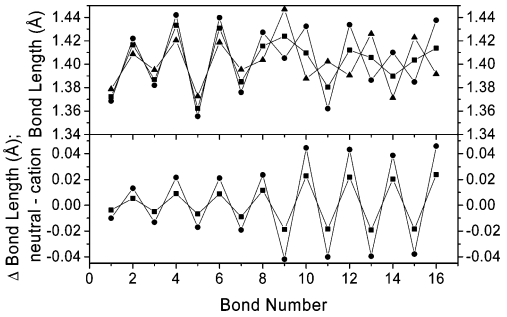

Figure 13. (a) Calculated bond lengths of the thienylenevinylene backbone of $(I\text{-}H/H)_2$ (●) and $(I\text{-}H/H)_2^{\bullet+}$ (■). (b) The changes in the bond lengths of the thienylenevinylene backbone of $(I\text{-}H/H)_2^{\bullet+}$ relative to the neutral dimer $(I\text{-}H/H)_2$. Calculated using the B3LYP/6-31G(d) method. The bond labeling system is shown in Figure 1.

will orient the charged defect toward the region of the thienylenevinylene backbone to which it is conjugated. That is to say, two distinct conjugation pathways are possible for the oxidized systems, involving either the aryl ethenyl substituent or bonds 1−8 of the thieneylene vinyelene backbone. However, both of these resonance structures direct the polaron defect over bonds 9−15, which are as such unaffected by the relative prominence of the two paths.

Analysis of the open-ended oxidation products requires consideration of the bond lengths of the σ-dimeric species. The bond alternation diagram for $(II\text{-}H)_2$, $(II\text{-}H)_2^{\bullet+}$, and $(II\text{-}H)_2^{2+}$ is presented in Figure 12a. The polaron is evidently delocalized over the entire structure. However, the terminal bonds lengthen by only 0.005 Å compared with 0.015 Å in the corresponding monomer $(II\text{-}Me)^{\bullet+}$ because the effects of the polaron are distributed over a longer conjugation length in the σ-dimer. The changes in bond length generally increase toward the center of the σ-dimer. A reversal of bond order is predicted for bonds 8 and 14 of the central four thiophene rings. The bond length data for $(II\text{-}H)_2^{2+}$ show increases in the magnitude of bond order reversal, with bond reversal predicted between the two equivalent bond 7's. Both charged defects appear to be distributed in a similar manner, i.e., concentrated toward the center of the conjugation length with a smooth transition through to the termini where the changes in bond length are minimal (Figure 12b).

The bond alternation diagrams for the substituted σ-dimers $(I\text{-}H/H)_2$ and $(I\text{-}H/H)^{\bullet+}$ are shown in Figure 13. They exhibit similar characteristics to the corresponding monomers in that the phenylethenyl moiety directs the charged defect away from bonds 1−8. For example, upon polaron formation, complete bond reversal is calculated for bonds 9 and 14, as opposed to bonds 8 and 14 for the unsubstituted $(II\text{-}H)_2^{\bullet+}$. This effect is also apparent when comparing the calculated changes in bond length of the polaron relative to the neutral species (Figure 13b). There is a noticeable difference in the magnitude of bond length change between the region that is conjugated to the phenylethenyl substituent (bonds 9−16) and that which is not (bonds 1−8). This demarcation is not predicted for the unsubstituted σ-dimers $(II\text{-}H)_2^{\bullet+}$ and $(II\text{-}H)_2^{2+}$ (Figure 12b), further evidence that the substituent orients the charged-defect toward the center of the conjugation path. This effect was found to be more prominent when electron donating substituents are present.

IV. Conclusion

We have investigated the spectroscopy and electronic structure of a series of ethylene-bridged thienylenevinylene oligomers with arylethenyl substituents on the central thiophene ring and with and without methyl α-end caps. The vibrational spectra (Raman and IR) are well modeled by DFT calculations with frequency MAD of 2−18 cm^{-1} for the compounds studied. From the structure calculations we find that there is a decrease in the bond length alternation of these bridged systems relative to the corresponding terthiophene compounds. This indicates that the ethylene bridges serve to increase the effective conjugation length and therefore enhance the delocalization of π-electrons. The experimental Raman spectra of these compounds are also consistent with an increase in delocalization of π-electrons with both line A and line B bands being at lower frequency in comparison to analogous terthiophene species. In addition to thiophene-based bands, the thienylenevinylene oligomers show bands attributed to the ethylene linkages in the thienylenevinylene backbone and due to the ethylene linkage in the arylethenyl groups.

The radical cations of the oligomers exhibit structural changes associated with charge localization at the central portion of the thienylenevinylene backbone; negligible structural changes are present on the arylethenyl substituent. This is manifest in both calculated structures and spectra and in experimental resonance Raman spectra, particularly the ethlylene stretching modes. However, the arylethenyl substituent is predicted to orientate the charged-defect toward regions of the thienylenevinylene conjugation path to which it is conjugated. This leads to higher spin densities at the head α-termini resulting in head-to-head σ-dimers with chemical or electrochemical oxidation. Furthermore, this leads to a partial confinement of the charged defect associated with cationic dimers, wherein the polaron structure is predominantly located between the two substituents. This effect is more pronounced in oligomers with stronger electron donating groups. The extent of defect delocalisation is thought to be critical to conduction, as such this type of study is essential to understanding the physical properties of conducting polymers and their function within electronic materials such as solar cells, organic light-emitting diodes and field effect transistors.

Acknowledgment. The support of the Foundation of Research Science and Technology (NERF), the Royal Society of New Zealand (Marsden Fund), and the MacDiarmid Institute for Advanced Materials and Nanotechnolgy is gratefully acknowledged.

References and Notes

(1) Pron, A.; Rannou, P. *Prog. Polym. Sci.* **2001**, *27*, 135.

(2) Gazotti, W. A.; Nogueira, A. F.; Girotto, E. M.; Micaroni, L.; Martini, M.; das Neves, S.; De Paoli, M. A. *Handbook of Advanced Electronic and Photonic Materials and Devices* **2001**, *10*, 53.

(3) Casado, J.; Miller, L. L.; Mann, K. R.; Pappenfus, T. M.; Kanemitsu, Y.; Orti, E.; Viruela, P. M.; Pou-Amerigo, R.; Hernandez, V.; Lopez, Navarrete, J. T. *J. Phys. Chem. B* **2002**, *106*, 3872.

(4) Casado, J.; Katz, H. E.; Hernandez, V.; Lopez, Navarrete, J. T. *J. Phys. Chem. B* **2002**, *106*, 2488.

(5) Garnier, F.; Horowitz, G.; Peng, X.; Fichou, D. *Adv. Mater.* **1990**, *2*, 592.

(6) Horowitz, G.; Garnier, F.; Yassar, A.; Hajlaoui, R.; Kouki, F. *Adv. Mater.* **1996**, *8*, 52.

(7) Garnier, F. *Chem. Phys.* **1998**, *227*, 253.

(8) Fichou, D.; Demanze, P.; Horowitz, G.; Hajlaoui, R.; Constant, M.; Garnier, F. *Synth. Met.* **1997**, *85*, 1309.

(9) Bredas, J. L.; Street, G. B. *Acc. Chem. Res.* **1985**, *18*, 309.

(10) Clarke, T. M.; Gordon, K. C.; Officer, D. L.; Grant, D. K. *J. Phys. Chem. A* **2005**, *109*, 1961.

(11) Grant, D. K.; Jolley, K. W.; Officer, D. L.; Gordon, K. C.; Clarke, T. M. *Org., Biomol. Chem.* **2005**, *3*, 2008.

(12) Clarke, T. M.; Gordon, K. C.; Officer, D. L.; Hall, S. B.; Collis, G. E.; Burrell, A. K. *J. Phys. Chem. A* **2003**, *107*, 11505.

(13) Casado, J.; Miller, L. L.; Mann, K. R.; Pappenfus, T. M.; Kanemitsu, Y.; Orti, E.; Viruela, P. M.; Pou-Amerigo, R.; Hernandez, V.; Navarrete, J. T. L. *J. Phys. Chem. B* **2002**, *106*, 3872.

(14) Roncali, J. *Chem. Rev.* **1997**, *97*, 173.

(15) Bredas, J. L. *J. Chem. Phys.* **1985**, *82*, 3808.

(16) Agosti, E.; Rivola, M.; Hernandez, V.; Del, Zoppo, M.; Zerbi, G. *Synth. Met.* **1999**, *100*, 101.

(17) Viruela, P. M.; Viruela, R.; Orti, E.; Casado, J.; Hernandez, V.; Lopez Navarrete, J. T. *J. Mol. Struct.* **2003**, *651*−*653*, 657.

(18) Wagner, P.; Ballantyne, A. M.; Jolley, K. W.; Officer, D. L. *Tetrahedron* **2006**, *62*, 2190.

(19) Furukawa, Y. *J. Phys. Chem.* **1996**, *100*, 15644.

(20) Louarn, G.; Buisson, J. P.; Lefrant, S.; Fichou, D. *J. Phys. Chem.* **1995**, *99*, 11399.

(21) Zerbi, G.; Chierichetti, B.; Ingaenas, O. *J. Chem. Phys.* **1991**, *94*, 4637.

(22) Roncali, J. *Chem. Rev.* **1992**, *92*, 711.

(23) Wintgens, V.; Valat, P.; Garnier, F. *J. Phys. Chem.* **1994**, *98*, 228.

(24) Helbig, M.; Hein, J.; Rentsch, S.; Burger, H.; Hobert, H. *Chem. Phys.* **1998**, *227*, 111.

(25) Howell, S. L.; Gordon, K. C. *J. Phys. Chem. A* **2004**, *108*, 2536.

(26) Matthewson, B. J.; Flood, A.; Polson, M. I. J.; Armstrong, C.; Phillips, D. L.; Gordon, K. C. *Bull. Chem. Soc. Jpn* **2002**, *75*, 933.

(27) Frisch, M. J.; Trucks, G. W.; Schlegel, H. B.; Scuseria, G. E.; Robb, M. A.; Cheeseman, J. R.; Montgomery, J. A., Jr.; Vreven, T.; Kudin, K. N.; Burant, J. C.; Millam, J. M.; Iyengar, S. S.; Tomasi, J.; Barone, V.; Mennucci, B.; Cossi, M.; Scalmani, G.; Rega, N.; Petersson, G. A.; Nakatsuji, H.; Hada, M.; Ehara, M.; Toyota, K.; Fukuda, R.; Hasegawa, J.; Ishida, M.; Nakajima, T.; Honda, Y.; Kitao, O.; Nakai, H.; Klene, M.; Li, X.; Knox, J. E.; Hratchian, H. P.; Cross, J. B.; Adamo, C.; Jaramillo, J.; Gomperts, R.; Stratmann, R. E.; Yazyev, O.; Austin, A. J.; Cammi, R.; Pomelli, C.; Ochterski, J. W.; Ayala, P. Y.; Morokuma, K.; Voth, G. A.; Salvador, P.; Dannenberg, J. J.; Zakrzewski, V. G.; Dapprich, S.; Daniels, A. D.; Strain, M. C.; Farkas, O.; Malick, D. K.; Rabuck, A. D.; Raghavachari, K.; Foresman, J. B.; Ortiz, J. V.; Cui, Q.; Baboul, A. G.; Clifford, S.; Cioslowski, J.; Stefanov, B. B.; Liu, G.; Liashenko, A.; Piskorz, P.; Komaromi, I.; Martin, R. L.; Fox, D. J.; Keith, T.; Al-Laham, M. A.; Peng, C. Y.; Nanayakkara, A.; Challacombe, M.; Gill, P. M. W.; Johnson, B.; Chen, W.; Wong, M. W.; Gonzalez, C.; Pople, J. A. *Gaussian 03*; Gaussian, Inc.: Pittsburgh, PA, 2003.

(28) Scott, A. P.; Radom, L. *J. Phys. Chem.* **1996**, *100*, 16502.

(29) Schaftenaar, G.; Noordik, J. H. *J. Computer-Aided Mol. Design* **2000**, *14*, 123.

(30) Manecke, G.; Haertel, M. *Chem. Ber.* **1973**, *106*, 655.

(31) Onoda, M.; Iwasa, T.; Kawai, T.; Yoshino, K. *J. Phys. D: Appl. Phys.* **1991**, *24*, 2076.

(32) Bouzzine, S. M.; Bouzakraoui, S.; Bouachrine, M.; Hamidi, M. *J. Mol. Struct. (THEOCHEM)* **2005**, *726*, 271.

(33) Casado, J.; Puig, J. J. M.; Hernandez, V.; Zotti, G.; Navarrete, J. T. L. *J. Phys. Chem. A* **2000**, *104*, 10656.

(34) Casado, J.; Hernandez, V.; Kanemitsu, Y.; Navarrete, J. T. L. *J. Raman Spectrosc.* **2000**, *31*, 565.

(35) Hernandez, V.; Casado, J.; Kanemitsu, Y.; Lopez, Navarrete, J. T. *J. Chem. Phys.* **1999**, *110*, 6907.

(36) Gordon, K. C.; MacArthur, S.; Clarke, T. M.; Officer, D. L.; Wagner, P. *J. Raman Spectrosc.* **2005**, *36*, 445.

(37) Hernandez, V.; Casado, J.; Ramirez, F. J.; Zotti, G.; Hotta, S.; Navarrete, J. T. L. *J. Chem. Phys.* **1996**, *104*, 9271.

(38) Furukawa, Y.; Akimoto, M.; Harada, I. *Synth. Met.* **1987**, *18*, 151.

(39) Clarke, T. M.; Gordon, K. C.; Officer, D. L.; Grant, D. K. *J. Chem. Phys.* **2006**, *124*, 164501.

(40) Grozema, F. C.; Van, Duijnen, P. T.; Siebbeles, L. D. A.; Goossens, A.; De Leeuw, S. W. *J. Phys. Chem. B* **2004**, *108*, 16139.